Research Article | Vol. 27, No. 9 | 29 Apr 2019 | OPTICS EXPRESS 12399
Optics EXPRESS

Simultaneous aberration and aperture control using a single spatial light modulator

NIKOLAI SUCHKOV,[1,2] ENRIQUE J. FERNÁNDEZ,[1,*] JOSE L. MARTÍNEZ-FUENTES,[3] IGNACIO MORENO,[3] AND PABLO ARTAL[1]

[1]*Laboratorio de Óptica, Centro de Investigación en Óptica y Nanofísica (CiOyN), Universidad de Murcia, Campus de Espinardo, 30010 Murcia, Spain*
[2]*Voptica S.L., Parque Científico de Murcia, Ctra. de Madrid 388, Complejo de Espinardo - Edificio S, 30100 Murcia, Spain*
[3]*Department of Material Science, Electronics, Optics and Technology, Universidad Miguel Hernández de Elche, 03202 Elche, Alicante, Spain*
[*]*enriquej@um.es*

Abstract: A method to simultaneously control aberrations and the aperture of an optical system using a single phase-only spatial light modulator was investigated. The experiment was performed using a liquid-crystal-on-silicon spatial light modulator (LCoS-SLM) within an adaptive optics system used for visual testing, although the method has broader applications in adaptive optics field. The performance of the technique was characterized through the estimation of the system's modulation transfer functions (MTFs) by using a random chart method. MTFs obtained from the phase modulation-based approach were compared with those from using a real aperture (diaphragm). The areas under the MTFs for the two conditions were similar up to 98%, confirming that the low-pass filter effect associated to the size of the entrance pupil was similar for the phase-modulated pupil and the physical pupil. As an example of application, both aberrations and pupil were controlled by a single phase-only modulator to study the through-focus visual performance in real subjects. Limitations and possible enhancements of the presented method were also discussed. The presented technique reduces complexity and cost of adaptive optics systems. It opens the door to new experiments by allowing dynamic modulation of aberrations and apertures of any shape.

1. Introduction

The ability to control both phase and amplitude of light is paramount to several fields in optics. Some of the applications include digital holography, wavefront shaping and adaptive optics (AO). In the case of AO it is particularly critical, as distribution of aberrations typically depends on the pupil of the system [1].

AO has found a natural field of application in visual science. For the last two decades, AO techniques have been widely employed both for imaging the eye and the retina [2–9], and for visual testing, using AO visual simulators (AOVS) [10–16]. Visual testing with AO permits understanding and characterizing the impact of optical quality of the eye on vision. For instance, it has been used to evaluate visual effects of correcting ocular aberrations [3, 4, 16–22], degradation of visual performance produced by individual aberrations [23–25], and the visual system's ability to adapt to monochromatic aberrations [26–28].

Liquid crystal spatial light modulators (LC SLM) have been used for aberration control in ophthalmic applications since late 1990s [3, 4]. LC SLMs present several advantages compared to other correcting devices, such as deformable mirrors. They allow for precise phase modulation due to their high spatial resolution, with a lower cost when compared to deformable mirrors [4–6]. High resolution of LC SLMs, typically above 1M of independent pixels, enables accurate wavefront modulation, and discontinuous and diffractive profiles can be programmed. Phase

#360306 https://doi.org/10.1364/OE.27.012399
© 2019 Received 15 Feb 2019; revised 20 Mar 2019; accepted 21 Mar 2019; published 17 Apr 2019

Optics EXPRESS

wrapping is usually required since phase variation of a liquid crystal is limited to a few wavelengths of amplitude. This might produce some diffraction effects, affecting the image quality [4]. LC-SLMs do not usually require closed loop operation due to their high stability, unlike many deformable mirrors [4–6], therefore simplifying control of the experiments. LC-SLMs have also been successfully used with polychromatic light [29]. They have been employed either as phase modulators for aberration control [14, 17, 24, 30, 31], or for amplitude modulation [32, 33]. In a study by Bowman et al. [34] an LC-SLM was also used for simultaneous measurement and control of aberrations. By manipulating the polarization of the incoming light, either phase or amplitude of the wavefront can be modulated. When they are employed for amplitude control, with an appropriate polarization setting of the incoming light, LC-SLMs can generate circular apertures of variable diameters, as well as free form pupil shapes [35].

It would be ideal to use a single LC-SLM to control both aperture and phase simultaneously, avoiding the need of changing the polarization state associated with each modality. An area where pupil size plays a major role is, again, visual optics. Contrast sensitivity and visual acuity [36], depth-of-focus [37–40] and accommodation [41, 42] are dependent on the pupil size. Vision through small apertures is even being used as an effective method to counteract presbyopia [43], as an example of practical application of pupil manipulation.

Some studies have demonstrated the feasibility of using a single device and polarization state to manipulate amplitude and phase. An early antecedent of the encoding of amplitude by using phase-only filters is found in Davis et al. [44]. Since then, different approaches have been explored to use an LC-SLM for independent and simultaneous phase and amplitude control. For instance, by using superpixel configurations with either two [45] or four [46] pixels, phase and amplitude control were decoupled from each other. Other studies [47, 48], employed an additional carrier spatial frequency to reduce diffraction efficiency of an SLM in the first diffraction order. These methods succeed in amplitude modulation in terms of reducing the intensity of the modulated light, and most of them have been devised in the context of computer-generated holography for the generation of customized laser beams. A useful review of the state-of-the-art can be found in Clark et al. [49].

In this work, we adapted a new encoding method [50], which allows for an independent control of phase and amplitude in the pupil plane using a single phase modulator and a single polarization state. It combines two functions: an axicon-shaped pupil mask that diverges the wavefront away from the axis, and the phase retardation induced by the liquid-crystal-on-silicon spatial light modulator (LCoS-SLM) inside of the pupil mask that results in phase modulation of the wavefront. This method presents the advantage of producing on-axis reconstruction of the complex function and therefore presents no loss of spatial bandwidth.

The manuscript is organized as follows. In the first section a description of the method to control the amplitude with phase masks will be provided. The method to test this approach will be based on estimation and comparison of the experimental modulation transfer functions (MTF), obtained both for phase masks and for physical diaphragms. Detailed description of how those functions were retrieved using an adaptive optics visual simulator (AOVS) will be given. The results will be presented in a separated section, together with an example of an application of the technique in the context of visual testing. A discussion on the limits of both the technique and the evaluation method will precede the conclusions of the work.

2. Methods

2.1. Pupil control using phase modulation

A brief summary of the encoding technique [50] is presented here. Let $F(\xi) = M(\xi)\exp(i\phi(\xi))$ be the complex valued pupil function to be encoded, where $M(\xi)$ and $\phi(\xi)$ represent the amplitude (pupil aperture) and phase (aberrations). In order to implement this complex function onto a phase-only LC SLM, a new multiplexed phase-only function $\exp(i\phi(\psi))$ is designed as described

Optics EXPRESS

in a different study [50]

$$\exp(i\psi(\xi)) = R(\xi)\exp(i\phi(\xi)) + \overline{R}(\xi)\exp(i\alpha(\xi)), \tag{1}$$

where $R(\xi)$ is a binary-amplitude (0-1) pattern, $\overline{R}(\xi)$ is its complementary pattern, and $\exp(i\alpha(\xi))$ is the phase function of a diverging element, a high frequency negative diffractive axicon, $\alpha(\xi) = -2\pi r/p$, r denoting the radial coordinate, and p – the axicon period.

The role of $R(\xi)$ is to select, at each pixel, between the aberration phase function $\phi(\xi)$ and the diverging axicon phase function $\alpha(\xi)$. The diffractive axicon acts as a circular blazed diffraction grating that diverges the light away from the optical axis. This way it encodes the amplitude information $M(\xi)$ onto the new multiplexed phase-only function $\psi(\xi)$.

If the required amplitude $M(\xi)$ is a binary function, the assignment $R(\xi) = M(\xi)$ is direct. However, the technique can incorporate amplitude levels through a random selection of the phase function that is applied at each pixel coordinate ξ. In this case, $R(\xi)$ is linked to the required amplitude $M(\xi)$ as

$$R(\xi) = \begin{cases} 1 & \text{if} \quad M(\xi) > \text{rnd}(\xi), \\ 0 & \text{if} \quad M(\xi) \leq \text{rnd}(\xi), \end{cases} \tag{2}$$

where $\text{rnd}(\xi)$ is a distribution of random numbers in the interval [0,1], one for each pixel.

This phase-only encoding technique of the complex function $M(\xi)\exp(i\phi(\xi))$ can be easily understood as follows. If the required amplitude $M(\xi)$ is close to 1, it is better represented by the phase-only function $\exp(i\phi(\xi))$ and $R(\xi) = 1$ is the good choice. On the contrary, for pixels where $M(\xi)$ is close to 0, light should be removed. The diverging axicon performs this operation directing light out of the optical axis. Therefore, $R(\xi) = 0$ is the right choice for these pixels. For intermediate values of $M(\xi)$, Eq. (2) provides an adequate random choice between the two phase-only functions. The random number approach is required when continuous amplitude levels are needed. However, in current application the mask is deterministic, as phase modulation is happening inside the hollow axicon mask without any transition or overlap, so no random number determination is necessary.

Axicon elements (both SLM-modulated and manufactured) have been widely used before for light manipulation. A more detailed description of their optical properties as well as applications can be found in other studies [51–55].

A detailed analysis of the accuracy of this encoding technique was provided in [50] for the implementation of digital holograms. In that work it was applied to the generation of higher order Laguerre-Gauss and Hermite-Gauss laser modes. Here, we study its performance in a completely different system, an adaptive optics visual simulator.

2.2. Experimental setup

For validation of the method, measurements were carried on using the setup shown in Fig. 1. The system was an adaptive optics visual simulator (AOVS), which general operation has been described in a different study [56]. The experimental setup allowed to perform both subjective and objective measurements, as described further.

Digital light processing projector (DLP) (DLPDLCR4710EVM-G2, Texas Instruments, Texas, USA), shown as DLP projector in Fig. 1, served as the stimuli generator in the experiment. The device is based on a digital micromirror device (DMD), which consists of an array of square micromirrors with a pitch of 5.4 μm. The images can be displayed at 1920 x 1080 resolution, refresh rate of 30 Hz, and a tunable luminous flux of up to 600 lm. The DMD is internally illuminated by three (R, G, B) light emitting diodes (LED). In order to reduce chromatic effects, a bandpass filter centered at 540 nm with a bandwidth of 10 nm, was used during the experiments [56]. It is possible to use a wider spectrum light with the described technique;

Optics EXPRESS

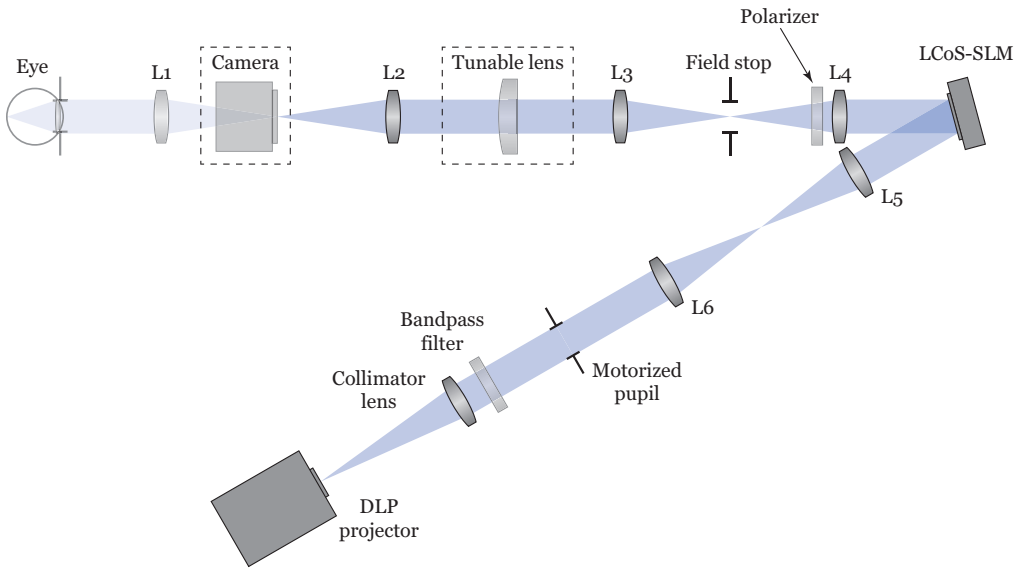

Fig. 1. Schematic of the system used in the experiment. L1 to L6 were achromatic doublets with focal length of 100 mm. For objective measurements, a camera was placed in the intermediate image plane between lenses L1 and L2. The tunable lens was removed. For visual operation, the camera was removed, while the tunable lens was inserted back in the plane between lenses L2 and L3. All the planes optically conjugated to the entrance pupil are shown with green color. Further explanations are provided in the text.

however, the diffraction efficiency would be decreased for wavelengths different from the design one. That happens due to an SLM being able to provide 2π phase modulation just for a single design wavelength, while for other wavelengths phase modulation would be either more or less than 2π, with other harmonic parasitic terms appearing. A study by Albero et al. [57] describes a way to adjust an SLM to provide a phase response closer to ideal 2π modulation for a given range of wavelengths. However, all those methods would result in additional complications compared to the monochromatic case.

An achromatic doublet with a focal length of 200 mm (collimator lens in Fig. 1) was placed in front of the DLP to produce an image at an infinite distance. Such a configuration results in an angular pixel size of 6 arc seconds at the system's entrance pupil.

A motorized pupil (8MID8.2-0.8-N, Standa Ltd, Vilnius, Lithuania) was placed in the focal plane of the collimator, which also corresponds to the Fourier plane of that lens. This plane contains the entrance pupil of the system, when light is propagating from the DLP to the eye. The physical pupil served to compare the performance of the pupil limited by the phase mask to the pupil limited by a physical aperture.

A telescope composed of two achromatic doublets with focal lengths of 100 mm (L5 and L6) was used to optically conjugate the entrance pupil plane to the liquid crystal-on-silicon spatial light modulator (LCoS-SLM), (PLUTO-VIS-014, Holoeye Photonics AG, Berlin, Germany). The LCoS-SLM employed in the experiment exhibits a full HD resolution (1920 x 1080) with a pixel pitch of 8 µm on a diagonal of 17.8 mm, and a fill factor of 93%. A rectangular field stop was placed in the intermediate image plane between lenses L3 and L4, limiting the field of view to 3.1 by 1.7 degrees. Linear polarizer was placed in front on lens L4 in order to filter the horizontally polarized light, parallel to the liquid crystal director axis. Location of the polarizer in the system doesn't affect the performance. However, in case the polarization axis doesn't

Optics EXPRESS

coincide with the liquid crystal director axis, the amount of non-modulated light rises, increasing energy in the zeroth order.

A telescope formed by the lenses L3 and L4 (both with f' = 100 mm) was used to conjugate the plane of the LCoS-SLM to an electrically tunable lens (TL) (Optotune EL-16-40-TC-VIS-20D, Optotune Switzerland AG, Dietikon, Switzerland). This element enabled manipulation of defocus independent of LCoS-SLM. The range of operation of the TL ran from -12 D to 10 D. During the retrieval of images for the objective evaluation of the technique the TL was off. The variable lens was solely used for the subjective measurements on real eyes to minimize the impact of the non-modulated light, as will be explained later in the next section. The last telescope, compounded by lenses L1 and L2 (both f' = 100 mm), relayed the plane of the TL to the plane of the subject's eye pupil.

It was important to consider the period of the axicon mask used for aperture modulation. As seen in Eq. (1) (and is discussed in detail in work of Martinez-Fuentes et al. [50]), the angular size of the image produced by the axicon depends on its period. Therefore, as the method was employed in a visual simulator system, it was beneficial to have the axicon-formed image as far from the optical axis as possible in order to mimic amplitude modulation. Because of this, a period of axicon of 3 pixels was used to have a large angle of deflection. A shorter period of only two pixels would result in a binary grating type axicon, thus leading to an equally intense converging axicon component, that would direct non-desired light into the optical axis.

Objective measurements involved recording of the images with an auxiliary CMOS camera (DMK 72AUC02, The Imaging Source Europe GmbH, Bremen, Germany) placed in the intermediate image plane between the lenses L1 and L2. The camera exhibited a resolution of 2592 x 1944 pixels, with a pixel pitch of 2.2 µm. The image size of a single DLP's micromirror on the camera was found to be 2.7 µm. Calibration of the system, including linearization of the TL and the LCoS-SLM was accomplished following a procedure described elsewhere [56]. The operation of the system was accomplished by dedicated software written in C++, while the processing of the experimental data was done using Matlab (Mathworks, Natick, MA, USA).

2.3. Experimental validation

The modulation transfer function (MTF) of the optical system was estimated to characterize the performance of the phase masks emulating pupils of different diameters. The MTF characterizes the attenuation in contrast of the spatial frequencies due to how these frequencies are transferred through an optical system. The MTF is an appropriate metric to investigate the effect of variable apertures, since both the cut-off frequency and the shape of the MTF change considerably as a function of the aperture diameter. Other possible metrics would be, for example, measuring optical aberration of the wavefront passing through the modulated aperture (as it would be dependent on the pupil diameter), or the total amount of light passing onto the image plane. However, former doesn't provide the information about contrast reduction and requires extra complexity for the optical system, as some form of wavefront sensing would be necessary; latter doesn't provide any information on spatial filtering effects of an aperture. The presence of aberrations is also a factor affecting the MTF. The AOVS was a near diffraction-limited system, except for the TL, which exhibited a moderate coma aberration for large pupils due to gravitational pull when positioned vertically regarding the ground plane. In order to avoid this, the TL was removed during the MTF retrieval.

The motorized pupil was kept in the plane conjugated to the LCoS-SLM. This diaphragm allowed to have ground-truth estimations of the MTF limited by a physical aperture, to be confronted with those obtained by phase manipulation.

For the retrieval of the MTF a technique based on the random chart method was used. This approach was first described in 1950s by Kubota et al. [58]. The method permits to calculate an MTF curve from a single measurement by using an extended white-noise single object. Previously

Optics EXPRESS

used with printed targets [59–61] or with a monitor [62], it was recently demonstrated to work with DMD-based object generator within the field of astronomical optics [63]. Provided that the AOVS incorporated a DMD-based projector, this method was chosen for the MTF estimation.

Briefly, the method requires a generation of a white noise object, with constant probability distribution. This is required for the object to exhibit a constant power spectral density (PSD). An image of the object is acquired through the optical system. Eventual inhomogeneities in the intensity distribution of the image arising from both the light source and the system must be accounted for as well. The averaged MTF of the system (MTF_{sys}) is then calculated by:

$$MTF_{sys}(\xi) = \sqrt{\frac{PSD_i(\xi) - PSD_w(\xi)}{PSD_o(\xi)}}, \tag{3}$$

where $PSD_i(\xi)$ is the PSD of the image of the white noise object, $PSD_w(\xi)$ is the PSD from the image of a white background (accounting for possible unequal intensity propagation), and $PSD_o(\xi)$ stands for power spectrum of the original object.

As the pixel of the camera was 2.2 µm, and the image of a single micromirror at the camera plane covered 2.7 µm, the object for MTF calculation was produced with 2x binning to satisfy the Nyquist criterion. In such case a single point of the binary pattern subtended 5.4 µm at the focal plane. The gap between the micromirrors was neglected assuming a 100% fill factor.

A set of baseline measurements was done with the motorized pupil at diameters of 2, 3, 4, 5 and 6 mm. The same diameters were later programmed on the LCoS-SLM by the appropriate phase masks. The motorized pupil was set at 7 mm, its maximum aperture, during the recording of the images produced with the phase masks limiting the pupil size. The object was limited to a square of 400 by 400 pixels. The impact of the size and the resolution of the object in the tested technique will be discussed with more detail in a separate section. An additional set of measurements was taken, combining the phase generation of pupils with additional defocus, all simultaneously programmed on the modulator solely by phase masks.

The object and its corresponding image through a phase mask corresponding to 3 mm pupil diameter are shown in Fig. 2.

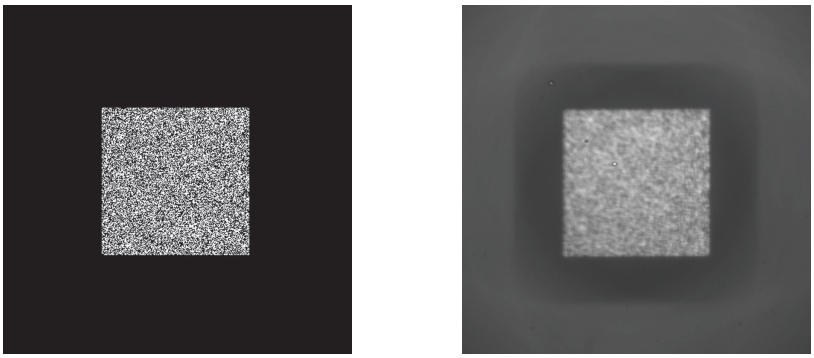

Fig. 2. Tested object and its image after passing through the phase mask corresponding to a pupil with a diameter of 3 mm. Left panel – object on the DLP, right panel – image on the camera.

In the second stage of the experiment, subjective measurements with real subjects were taken as an example of application of the technique in the AOVS to study vision. Simultaneous control of defocus and pupil size through phase-only manipulation was tested on two subjects. The subjects were nearly emmetropic healthy adults (43 and 45 years old), without any optical aid for far vision. Both were experienced subjects in visual testing and familiar with the experiment.

Optics EXPRESS

Cycloplegics were instilled in the eye in order to paralyze the remaining accommodation and dilate the pupil.

A gray level representation of the phase displayed on the modulator is presented in Fig. 3. The auxiliary camera to record the images from the DLP was removed from the system. The TL was put back in the plane between lenses L2 and L3 (as shown in Fig. 1).

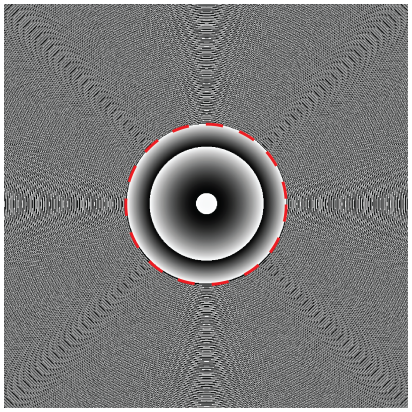

Fig. 3. Phase mask used for simultaneous phase modulation and pupil control. Red dashed circle shows the separation of the two zones. Inside the circle – phase modulation, in this case induced defocus. Outside the circle – phase mask used for controlling the size of the pupil, changing the amplitude of the image.

Since the LCoS-SLM does not have a diffraction efficiency of 100%, there is always a fraction of light which passes through the system non-modulated. Under certain circumstances, especially when large values of aberrations are programmed, the non-modulated light might form an image brighter than the aberrated image. To prevent this, a constant 2 D defocus offset was introduced with the LCoS-SLM. The off-set was subsequently accounted for by the TL, which also incorporated the subject's refraction. TL was also used to manipulate the through focus conditions. This resulted in the non-modulated portion of light always being defocused, while modulated light stayed in focus.

The experimental procedure was as follows: the subjects were aligned in the system and corrected for their refraction with the AOVS. The refraction was estimated from their wavefronts, which were retrieved by the Hartmann-Shack sensor available in the AOVS. High contrast visual acuity (VA) was acquired through focus for two pupil sizes: 2 and 6 mm of diameter. Through focus conditions sampling a 4 D range around the best correction were programmed on the modulator. For the larger pupil size, simultaneous full aberration correction (up to the 6^{th} order) was set in the modulator. VA was measured every 0.5 D for each condition. For determining VA, the Freiburg test [64] was used with a white E letter of varying size on a black background, with 90 trials for each VA estimation. The raw data from the VA test was fitted to a sigmoid function, with the threshold set at 75% of correct answers.

3. Results

3.1. Objective measurements

The images of the white noise object transmitted through the system were recorded and analyzed following the procedure described in previous section for 5 pupil sizes. The images were taken with both the physical pupil and with the pupil generated by the phase mask on the LCoS-SLM. Figure 4 graphically shows the results. In all cases, curves corresponding to the diffraction

Optics EXPRESS

limited case for the same circular pupil diameter are shown for reference. The obtained MTFs were radially averaged and calculated from the entire field of the binary object.

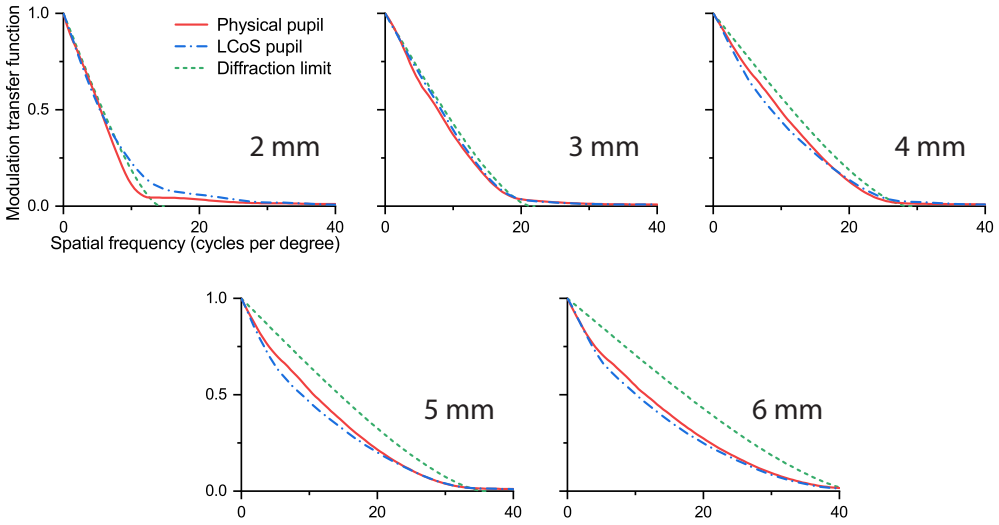

Fig. 4. Modulation transfer functions (MTFs) produced by the physical pupil and by the LCoS-SLM modulated pupil for different pupil sizes. Diffraction limited MTF for each pupil size is shown for reference.

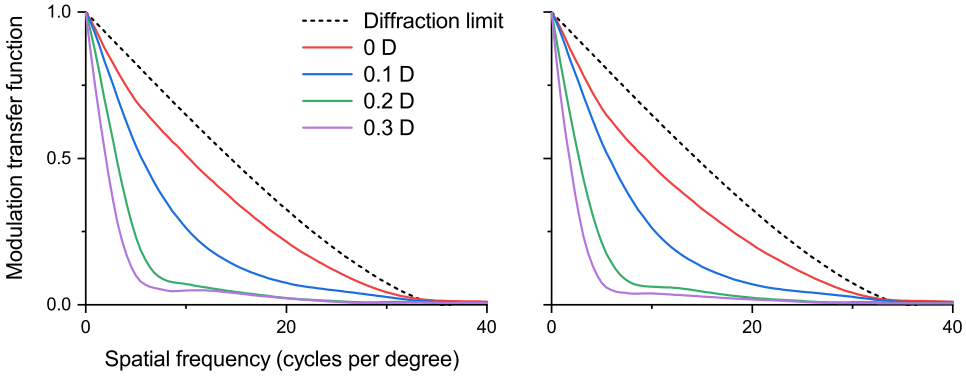

Fig. 5. MTF curves for simultaneous control of pupil size and phase. Left panel represents the case when pupil is controlled by a motorized iris with defocus modulated on the LCoS-SLM, while right panel shows the case with the LCoS-SLM controlling both defocus and pupil diameter.

The MTF curves obtained for pupils produced by both the real aperture and the LCoS-SLM present a significant resemblance along the range at every pupil size. This is a qualitative indicator that the phase-generated pupil performs like a physical aperture. It can be noted that the MTF curves for physical pupils of 2 and 3 mm are very similar to the diffraction limited MTF. As the diameter of the considered pupil increases, the experimental curves separate from the diffraction limited case. This fact is very likely related with the progressive increase of aberrations as the pupil expands. In order to provide the reader with numerical values to characterize the similarity

Optics EXPRESS

of the MTF curves, the area under the curve was obtained for each case. For pupil diameters of 3 to 6 mm, the difference between areas under the MTF for LCoS-SLM and physical pupil are below 2%. For the case of 2 mm pupil, the difference between MTF areas reaches 8%.

Having validated that the pupil diameter can be modulated using the LCoS-SLM, pupil modulation was combined with defocus modulation. MTF curves with induced defocus are shown in Fig. 5. Defocus was solely controlled by the LCoS-SLM in both cases, while pupil size was constricted by the motorized pupil in one case, and by the LCoS-SLM in the other. For this case a pupil diameter of 5 mm was selected.

Comparing the areas under the MTF curves for identical defocus, the difference between the LCoS-SLM and the physical pupil was below 2% at every condition. Larger defocus might compromise the retrieval of MTF using the proposed method, as will be discussed in a separate section.

3.2. *Visual simulation experiments*

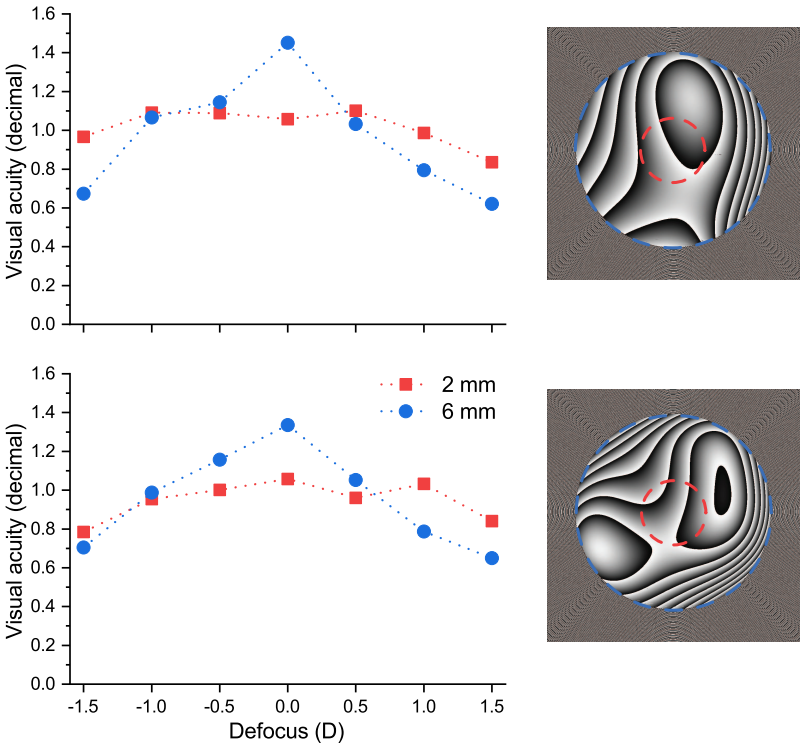

Fig. 6. VA through focus for two pupil sizes. Top row – subject S1, bottom – subject S2. The right panels show the phase mask corresponding to the pupil of 6 mm with the correction of the aberrations (inside the blue dashed circle). Red dashed circles indicate the 2 mm pupil.

In this section an example of practical application of the method in the context of vision is provided. Simultaneous manipulation of phase and pupil size by the modulator is employed to acquire the through focus visual response in two subjects. The high contrast VA was estimated following the procedure described before for pupil diameters of 2 and 6 mm. Full aberration correction was applied for the 6 mm pupil size. The results are presented in Fig. 6.

As seen in Fig. 6, the VA curves for the case of the 2 mm pupil are lower for the in-focus position and flatter overall, when compared to the 6 mm pupil. For subject JF the difference

Optics EXPRESS

between peak VA values was 0.394 decimal, while for subject EV the difference was 0.278 decimal. The depth-of-field increase for smaller pupil diameter is consistent with previous studies [38, 40, 65], indicating that the method performed correctly for this visual application.

4. Discussion

Presented approach to simultaneously drive the pupil and the aberrations by using a single liquid-crystal phase-only modulator offers several advantages. Those are particularly important in contexts where both the pupil and the aberrations must be controlled independently. Pupil of the eye is known to change, among other causes, as a function of luminance, vergence and accommodation [66, 67], showing the importance of the presented study to visual optics field. Technique which was proposed and tested in this work avoids the use of variable diaphragms or motorized components in the system, therefore reducing its complexity and cost. As the SLM is only used to display a phase mask, part of which mimics amplitude modulation, setup is simplified significantly compared to the cases when an extra SLM is used for true amplitude modulation, where a separate polarization state is required [21, 33]. In addition, the method also enables generation of other pupil shapes, such as elliptical ones or of even more exotic geometries, which might be of interest for designing novel ophthalmogical solutions, as shown in a different study [35].

Other techniques can be used to replicate the effect of mimicking amplitude modulation using a phase-only element. For example, a diffractive grating can be used for diverging the light out of the optical axis, as demonstrated in a study by Arrizón [68]. However, compared to that technique, an axicon is better suited to a rotational symmetry, which is necessary for visual applications. A diverging lens can also be used for the same effect. Axicon, grating or diverging lens elements can also be fabricated as Pancharatnam-Berry phase elements, but they cannot be programmed on an SLM.

Retrieved MTFs characterized the method of simultaneous phase and aperture control and provided a complete picture of its performance. Direct comparison between the MTFs obtained through a physical pupil and a phase generated pupil was accomplished. We employed a revisited method involving Fourier analysis, by generating a white noise object to be imaged through the system, which can be successfully applied with current DLP technologies. One important advantage of DLP based devices is the excellent contrast attainable between adjacent pixels in the object, as the black pixels are produced by diverging the light out of the main path. The resolution of the DLP is also advantageous for the MTF estimation. In fact, a 2x binning resolution reduction on the DLP was applied to prevent aliasing effect on the camera sensor. Still, the method to estimate the MTF is affected by some constrains. It should be noted that the obtained MTF is calculated from an extended object, so it is weighted across certain field. This does not occur when MTF is obtained from a point spread function of the system. This fact causes MTF to vary depending on the size of the object. In this work a relatively small field was used. Even though it was around 0.5 degrees, some amount of field curvature was present, affecting the measurements. That was the most prominent aberration, since on-axis aberrations were measured during the calibration of the system, and it maintained a nearly diffraction-limited optical quality. Field curvature in the system was mainly due to the use of a single achromatic lens as collimator. More complex objectives compounded by several elements are typically employed to avoid this aberration. This effect explains the drop of the experimental MTF below the diffraction limit for diameters of 4 mm and larger. Nevertheless, comparison between the real pupil and the one generated with phase manipulation still stands, as both cases are affected by the same field curvature. Another limitation of the random chart MTF retrieval method is the range of aberrations that can be introduced in the system. Highly aberrated systems, not necessarily with high order aberrations, but with a simple defocus, produce a known effect of low pass filtering over the spatial frequencies. The white noise object method to estimate the

Optics EXPRESS

MTF would accordingly require larger images. But in such case field aberrations would likely become predominant. Therefore, there must be a balance when applying the method, which would depend on characteristics of the system which needs to be evaluated.

A limitation of the method to generate pupils by manipulating phase is connected to the field size in the object space. The phase mask generated a ring as a collateral effect associated to the period of the axicon-shaped mask. That can be observed in the right panel of Fig. 2 and in Fig. 7. The ring size, as shown in Fig. 7, is directly connected to the size of the object, or the total field. For a certain object field size, the ring overlaps with the image. This overlapping does not affect the intended pupil effect in terms of the spatial cut-off frequency, as the ring does not cause additional high spatial frequencies to be transferred to the image. However, this fact might impact the performance, since it introduces some extra scatter, consequently reducing the contrast of the images, as graphically shown in Fig. 7.

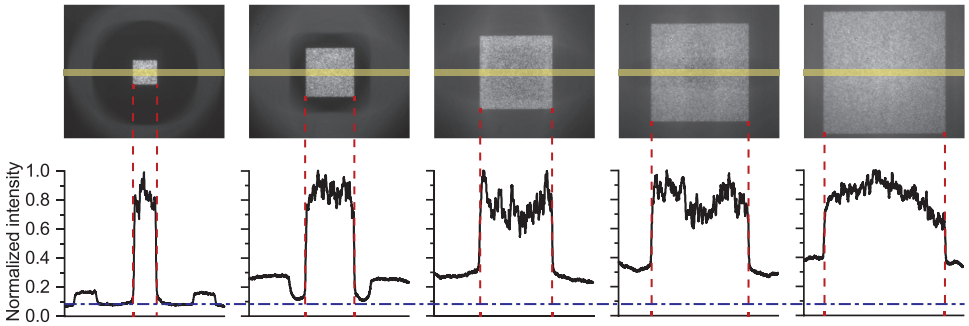

Fig. 7. Effect of different object sizes on the image. Top row, from left to right, images of the object subtending: 200, 400, 600, 800 and 1000 pixels. Bottom row: normalized averaged intensity of yellow shaded parts. Red dashed lines show borders of the object. Blue dashed line shows the background intensity.

This overlapping effect also depends on the configuration of the system through the magnification between conjugate planes. In the experiment, magnification was set to |1|. Reducing the magnification factor on the plane of the phase modulator would permit using a larger object. The diameter of the ring can be increased, reducing its impact on the image quality, by reducing the physical period of the axicon phase mask. That can be accomplished by using a spatial light modulator with smaller pixel pitch. Axicon phase mask with a period subtending the same amount of pixels would be used, but a reduced physical period size would result in a higher deflection angle, producing a ring of larger diameter. In this regard, there are off-the-shelf modulators with 4K resolution with similar chip size.

Another aspect to be accounted for when using the proposed technique is the ratio between the diameter of the incoming beam and the programmed pupil diameter. This is important due to the amount of light that is not modulated. The following expression accounts for the ratio between non-modulated and modulated fractions of the incoming light k_{nonmod} (assuming circular pupils):

$$k_{nonmod} = (1 - \nu) \cdot \frac{R_t^2 - R_p^2}{R_p^2}, \tag{4}$$

where ν is diffractive efficiency of the modulator, R_t is the radius of the incoming light, R_p is the radius of the modulated pupil.

As an example, assuming a typical commercial value of an LCoS-SLM's diffractive efficiency of 95%, the ratio k_{nonmod} reaches a value of 0.15 when the modulated pupil is 2 times smaller than the incoming beam, of 0.75 when 4 times smaller and of 3.15 when 8 times smaller. Due to

Optics EXPRESS

this, if small diameters of the pupil are produced by the modulator, it is recommended that the incoming beam is limited by a physical aperture before the LCoS-SLM. However, this issue can be overcome by introducing an offset in phase on the LCoS-SLM, for instance defocus, as it has been explained in previous section about the visual testing experiment. Introducing a tunable lens for offset compensation is not strictly necessary, as the defocus offset programmed on the LCoS-SLM can be compensated in the system by altering one of the telescopes, or, alternatively, by moving the object away from the focal plane of the collimating lens. Such configurations guarantee that the non-modulated fraction of light will always be defocused on the image plane (e.g. an observer's retina or a camera detector).

Inducing aberrations together with the pupil control was experimentally demonstrated by generating defocus up to 0.3 D of amplitude for the objective measurements (limited by the MTF retrieval technique), and up to 4 D for the visual application. It must be pointed out that the ring around the image produced by the axicon mask does not depend on the programmed aberrations. This is graphically shown in Fig. 8, where defocus up to 8 D through a pupil of 5 mm was generated by the LCoS-SLM.

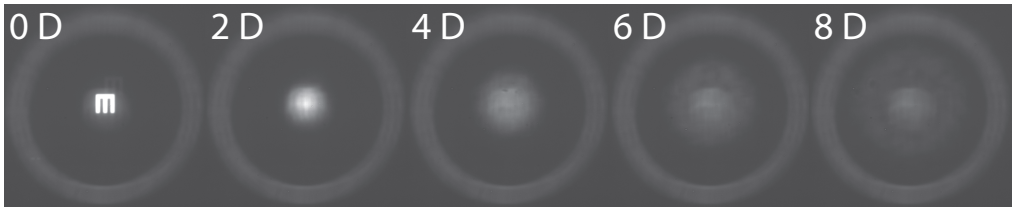

Fig. 8. Image of E letter for different values of defocus. Pupil of 5 mm in diameter is modulated on the LCoS-SLM. Images are overexposed in order to highlight the ring produced by the aperture mask, which keeps its size constant, independent of the induced defocus.

The E letter shown in Fig. 8 subtends approximately 10 arc minutes, corresponding to VA of 0.5 decimal. The intensity of the ring in the focal plane remains constant, as it depends on the size of the aperture mask relative to the size of the oncoming beam.

5. Conclusion

A new method to dynamically manipulate the aperture of an optical system simultaneously with the aberration control has been investigated in the context of visual adaptive optics simulation. Technique employs phase modulation of the incoming light to create an effect of a physical pupil. Consequently both aperture and phase can be driven with a single liquid-crystal phase-only modulator. Technique has been experimentally tested through the comparison of MTFs obtained with the phase-only approach and physical diaphragm apertures. Measurements were done using an AOVS. Limitations and enhancements of the technique have been discussed in detail. As an example of an application, through focus VA was obtained in 2 subjects using different pupil sizes and performing full aberration correction.

Simultaneous control of aperture and phase by using a single phase modulator is very relevant for adaptive optics visual simulation. Visual testing can largely benefit from this technique, as both aberrations and pupil size affect the optical quality of retinal images. The application of this technique opens the door to new experiments under realistic conditions to better understand vision, and to the design of novel optical aids combining pupil and phase engineering. Presented technique also has applications in adaptive optics field in general.

Optics EXPRESS

Funding

European Union's Horizon 2020 Marie Sklodowska-Curie grant (MyFUN, 675137); European Research Council Advanced Grant (SEECAT) (ERC-2013-AdG-339228); Secretaría de Estado de Investigación, Desarrollo e Innovación (SEIDI) (FIS2016-76163-R); Fundación Séneca - Agencia de Ciencia y Tecnología de la Región de Murcia (19897/GERM/15, 20513/PDC/18); European Regional Development Fund (EU-FEDER); Generalitat Valenciana, Conselleria d'Educació, Investigación, Cultura i Esport (PROMETEO-2017-154).

Acknowledgments

The authors thank Javier Roca for developing parts of the software to control the instrument and Marcos Herreras for some laboratory work.

References

1. J. Y. Wang and D. E. Silva, "Wave-front interpretation with Zernike polynomials," Appl. Opt. **19**, 1510–1518 (1980).
2. J. Liang, D. R. Williams, and D. T. Miller, "Supernormal vision and high-resolution retinal imaging through adaptive optics," J. Opt. Soc. Am. A **14**, 2884–2892 (1997).
3. H. Hofer, L. Chen, G. Y. Yoon, B. Singer, Y. Yamauchi, and D. R. Williams, "Improvement in retinal image quality with dynamic correction of the eye's aberrations," Opt. Express **8**, 631–643 (2001).
4. N. Doble, G. Yoon, L. Chen, P. Bierden, B. Singer, S. Olivier, and D. R. Williams, "Use of a microelectromechanical mirror for adaptive optics in the human eye," Opt. Lett. **27**, 1537–1539 (2002).
5. E. J. Fernández and P. Artal, "Membrane deformable mirror for adaptive optics: performance limits in visual optics," Opt. Express **11**, 1056–1069 (2003).
6. D. T. Miller, L. N. Thibos, and X. Hong, "Requirements for segmented correctors for diffraction-limited performance in the human eye," Opt. Express **13**, 275–289 (2005).
7. E. Dalimier and C. Dainty, "Comparative analysis of deformable mirrors for ocular adaptive optics," Opt. Express **13**, 4275–4285 (2005).
8. E. J. Fernández, A. Unterhuber, B. Považay, B. Hermann, P. Artal, and W. Drexler, "Chromatic aberration correction of the human eye for retinal imaging in the near infrared," Opt. Express **14**, 6213–6225 (2006).
9. E. J. Fernández and P. Artal, "Ocular aberrations up to the infrared range: from 632.8 to 1070 nm," Opt. Express **16**, 21199–21208 (2008).
10. E. J. Fernández, "Adaptive Optics for Visual Simulation," ISRN Opt. **2012**, 1–13 (2012).
11. S. Manzanera, P. M. Prieto, D. B. Ayala, J. M. Lindacher, and P. Artal, "Liquid crystal Adaptive Optics Visual Simulator: Application to testing and design of ophthalmic optical elements," Opt. Express **15**, 16177–16188 (2007).
12. C. Schwarz, P. M. Prieto, E. J. Fernández, and P. Artal, "Binocular adaptive optics vision analyzer with full control over the complex pupil functions," Opt. Lett. **36**, 4779–4781 (2011).
13. E. J. Fernández, L. Vabre, B. Hermann, A. Unterhuber, B. Považay, and W. Drexler, "Adaptive optics with a magnetic deformable mirror: applications in the human eye," Opt Express **14**, 8900–8917 (2006).
14. E. J. Fernández, P. M. Prieto, and P. Artal, "Wave-aberration control with a liquid crystal on silicon (LCOS) spatial phase modulator," Opt. Express **17**, 11013–11025 (2009).
15. E. J. Fernández, I. Iglesias, and P. Artal, "Closed-loop adaptive optics in the human eye," Opt. Lett. **26**, 746–748 (2001).
16. L. N. Thibos and A. Bradley, "Use of Liquid-Crystal Adaptive-Optics to Alter the Refractive State of the Eye," Optom. Vis. Sci. **74**, 581–587 (1997).
17. F. Vargas-Martín, P. M. Prieto, and P. Artal, "Correction of the aberrations in the human eye with a liquid-crystal spatial light modulator: limits to performance," J. Opt. Soc. Am. A **15**, 2552–2562 (1998).
18. L. Chen, P. B. Kruger, H. Hofer, B. Singer, and D. R. Williams, "Accommodation with higher-order monochromatic aberrations corrected with adaptive optics," J. Opt. Soc. Am. A **23**, 1–8 (2006).
19. E. A. Rossi, P. Weiser, J. Tarrant, and A. Roorda, "Visual performance in emmetropia and low myopia after correction of high-order aberrations," J. Vis. **7**(8), 14 (2007).
20. S. Marcos, L. Sawides, E. Gambra, and C. Dorronsoro, "Influence of adaptive-optics ocular aberration correction on visual acuity at different luminances and contrast polarities," J. Vis. **8**(13), 1 (2008).
21. C. Schwarz, S. Manzanera, P. M. Prieto, E. J. Fernández, and P. Artal, "Comparison of binocular through-focus visual acuity with monovision and a small aperture inlay," Biomed. Opt. Express **5**, 3355–3366 (2014).
22. L. Sawides, E. Gambra, D. Pascual, C. Dorronsoro, and S. Marcos, "Visual performance with real-life tasks under Adaptive-Optics ocular aberration correction," J. Vis. **10**(5), 19 (2010).
23. K. M. Rocha, L. Vabre, N. Chateau, and R. R. Krueger, "Expanding depth of focus by modifying higher-order aberrations induced by an adaptive optics visual simulator," J. Cataract. & Refract. Surg. **35**, 1885–1892 (2009).
24. E. J. Fernández, P. M. Prieto, and P. Artal, "Binocular adaptive optics visual simulator," Opt. Lett. **34**, 2628–2630 (2009).

Optics EXPRESS

25. E. A. Villegas, E. Alcón, S. Mirabet, I. Yago, J. M. Marín, and P. Artal, "Extended Depth of Focus With Induced Spherical Aberration in Light-Adjustable Intraocular Lenses," Am. J. Ophthalmol. **157**, 142–149 (2014).
26. P. Artal, L. Chen, E. J. Fernández, B. Singer, S. Manzanera, and D. R. Williams, "Neural compensation for the eye's optical aberrations," J. Vis. **4**, 281–287 (2004).
27. L. Chen, P. Artal, D. Gutierrez, and D. R. Williams, "Neural compensation for the best aberration correction," J. Vis. **7**(10), 9 (2007).
28. L. Sawides, S. Marcos, S. Ravikumar, L. N. Thibos, A. Bradley, and M. Webster, "Adaptation to astigmatic blur," J. Vis. **10**(12), 22 (2010).
29. J. L. Martinez, E. J. Fernández, P. M. Prieto, and P. Artal, "Chromatic aberration control with liquid crystal spatial phase modulators," Opt. Express **25**, 9793–9801 (2017).
30. C. Cánovas, P. M. Prieto, S. Manzanera, A. Mira, and P. Artal, "Hybrid adaptive-optics visual simulator," Opt. Lett. **35**, 196–198 (2010).
31. P. M. Prieto, E. J. Fernández, S. Manzanera, and P. Artal, "Adaptive optics with a programmable phase modulator: applications in the human eye," Opt. Express **12**, 4059–4071 (2004).
32. C. Schwarz, S. Manzanera, P. M. Prieto, P. Piers, P. Artal, C. Cánovas, and H. Weeber, "Binocular visual acuity for the correction of spherical aberration in polychromatic and monochromatic light." J. Vis. **14**, 1–11 (2014).
33. S. Manzanera, P. M. Prieto, A. Benito, J. Tabernero, and P. Artal, "Location of Achromatizing Pupil Position and First Purkinje Reflection in a Normal Population," Investig. Ophthalmol. & Vis. Sci. **56**, 962–966 (2015).
34. R. W. Bowman, A. J. Wright, and M. J. Padgett, "An SLM-based Shack-Hartmann wavefront sensor for aberration correction in optical tweezers," J. Opt. **12**, 124004 (2010).
35. A. Radhakrishnan, C. Dorronsoro, and S. Marcos, "Differences in visual quality with orientation of a rotationally asymmetric bifocal intraocular lens design," J. Cataract. & Refract. Surg. **42**, 1276–1287 (2016).
36. F. W. Campbell and A. H. Gregory, "Effect of Size of Pupil on Visual Acuity," Nature **187**, 1121–1123 (1960).
37. F. Campbell, "The Depth of Field of the Human Eye," Opt. Acta: Int. J. Opt. **4**, 157–164 (1957).
38. K. N. Ogle and J. T. Schwartz, "Depth of Focus of the Human Eye," J. Opt. Soc. Am. **49**, 273–280 (1959).
39. D. A. Atchison, W. N. Charman, and R. L. Woods, "Subjective Depth of Focus of the Eye," Optom. Vis. Sci. **74**, 511–520 (1997).
40. B. Wang and K. J. Ciuffreda, "Depth-of-Focus of the Human Eye: Theory and Clinical Implications," Surv. Ophthalmol. **51**, 75–85 (2006).
41. R. T. Hennessy, T. Iida, K. Shiina, and H. Leibowitz, "The effect of pupil size on accommodation," Vis. Res. **16**, 587–589 (1976).
42. B. Winn, D. Whitaker, D. B. Elliott, and N. J. Phillips, "Factors affecting light-adapted pupil size in normal human subjects." Investig. Ophthalmol. Vis. Sci. **35**, 1132–1137 (1994).
43. E. J. Fernández, C. Schwarz, P. M. Prieto, S. Manzanera, and P. Artal, "Impact on stereo-acuity of two presbyopia correction approaches: monovision and small aperture inlay," Biomed. Opt. Express **4**, 822–830 (2013).
44. J. A. Davis, D. M. Cottrell, J. Campos, M. J. Yzuel, and I. Moreno, "Encoding amplitude information onto phase-only filters," Appl. Opt. **38**, 5004–5013 (1999).
45. V. Arrizón, "Complex modulation with a twisted-nematic liquid-crystal spatial light modulator: double-pixel approach," Opt. Lett. **28**, 1359–1361 (2003).
46. E. G. van Putten, I. M. Vellekoop, and A. P. Mosk, "Spatial amplitude and phase modulation using commercial twisted nematic LCDs," Appl. Opt. **47**, 2076–2081 (2008).
47. J. A. Davis, K. O. Valadéz, and D. M. Cottrell, "Encoding amplitude and phase information onto a binary phase-only spatial light modulator," Appl. Opt. **42**, 2003–2008 (2003).
48. V. Bagnoud and J. D. Zuegel, "Independent phase and amplitude control of a laser beam by use of a single-phase-only spatial light modulator," Opt. Lett. **29**, 295–297 (2004).
49. T. W. Clark, R. F. Offer, S. Franke-Arnold, A. S. Arnold, and N. Radwell, "Comparison of beam generation techniques using a phase only spatial light modulator," Opt. Express **24**, 6249–6264 (2016).
50. J. L. Martínez Fuentes and I. Moreno, "Random technique to encode complex valued holograms with on axis reconstruction onto phase-only displays," Opt. Express **26**, 5875–5889 (2018).
51. Q. Ren and R. Birngruber, "Axicon : A New Laser Beam Delivery System for Corneal Surgery," J. Quantum Electron. **26**, 2305–2308 (1990).
52. N. Davidson, A. A. Friesem, and E. Hasman, "Holographic axilens: high resolution and long focal depth." Opt. letters **16**, 523–525 (1991).
53. V. V. Kotlyar, A. A. Kovalev, R. V. Skidanov, O. Y. Moiseev, and V. A. Soifer, "Diffraction of a finite-radius plane wave and a Gaussian beam by a helical axicon and a spiral phase plate," J. Opt. Soc. Am. A **24**, 1955–1964 (2007).
54. J. H. Wirth, A. T. Watnik, and G. A. Swartzlander, "Experimental observations of a laser suppression imaging system using pupil-plane phase elements," Appl. Opt. **56**, 9205–9211 (2017).
55. J. Ren, W. Wang, and W. Yang, "Micro-patterned liquid crystal Pancharatnam-Berry axilens," Chin. Opt. Lett. **16**, 062301 (2018).
56. N. Suchkov, E. J. Fernández, and P. Artal, "Wide-range adaptive optics visual simulator with a tunable lens," J. Opt. Soc. Am. A, accepted for publication (2019).
57. J. Albero, I. Moreno, and J. Campos, "Enhancement of the broadband modulation diffraction efficiency of liquid-crystal displays," Opt. Lett. **37**, 52–54 (2012).

Optics EXPRESS

58. H. Kubota and H. Ohzu, "Method of Measurement of Response Function by Means of Random Chart," J. Opt. Soc. Am. **47**, 666–667 (1957).
59. A. Daniels, G. D. Boreman, A. D. Ducharme, and E. Sapir, "Random transparency targets for modulation transfer function measurement in the visible and infrared regions," Opt. Eng. **34**, 860–868 (1995).
60. Q. H. Hong, A. H. Lettington, and J. Macdonald, "Measuring the MTF for focal plane arrays using random noise targets," Meas. Sci. Technol. **7**, 1087–1091 (1996).
61. S. M. Backman, A. J. Makynen, T. T. Kolehmainen, and K. M. Ojala, "Random target method for fast MTF inspection," Opt. Express **12**, 2610–2615 (2004).
62. E. Levy, D. Peles, M. Opher-Lipson, and S. G. Lipson, "Modulation transfer function of a lens measured with a random target method," Appl. Opt. **38**, 679–683 (1999).
63. A. Travinsky and Z. Ninkov, "Measurement of Modulation Transfer Function using Digital Micromirror Devices," in *Imaging and Applied Optics,* vol. 2018 (2018), pp. 1–2.
64. M. Bach, "The Freiburg Visual Acuity Test - Automatic Measurement of Visual Acuity," Optom. Vis. Sci. **73**, 49–53 (1996).
65. S. Marcos, E. Moreno, and R. Navarro, "The depth-of-field of the human eye from objective and subjective measurements," Vis. Res. **39**, 2039–2049 (1999).
66. H. Ripps, N. B. Chin, I. M. Siegel, and G. M. Breinin, "The effect of pupil size on accommodation, convergence, and the AC/A ratio," Investig. ophthalmology **1**, 127–135 (1962).
67. S. G. de Groot and J. W. Gebhard, "Pupil Size as Determined by Adapting Luminance," J. Opt. Soc. Am. **42**, 492–495 (1952).
68. V. Arrizón, "Optimum on-axis computer-generated hologram encoded into low-resolution phase-modul ation devices," Opt. Lett. **28**, 2521–2523 (2007).